Centimetric CrSi2 crystal grown by the vertical gradient Freeze method

A. Moll, S. Laborde, F. Barou, Mickael Beaudhuin

Version of Record: https://www.sciencedirect.com/science/article/pii/S0022024820300282
Manuscript_d11e4d7599bf0c8481dfd1bd9d32e48b

Centimetric $CrSi_2$ crystal grown by the Vertical Gradient Freeze method

A. Moll[a] *, S. Laborde[a], F. Barou[b], M. Beaudhuin[a] *

[a] ICGM, Univ Montpellier, CNRS, ENSCM, Montpellier, France

[b] Géosciences Montpellier, Univ. Montpellier, CNRS, Montpellier, France

*** corresponding authors: moll.adrien@orange.fr, mickael.beaudhuin@umontpellier.fr**

Abstract

$CrSi_2$ ingots were grown by the Vertical Gradient Freeze (VGF) method in silica (SiO_2) crucibles with boron nitride (BN) coating and in pyrolytic boron nitride (pBN) crucibles in order to minimize the sticking and the reaction with the molten Cr-Si alloy. High quality chromium disilicide single crystal was obtained with a mosaicity of 1 to 2° using pBN crucible with a thermal gradient of 0.6 K/mm and a growth rate of 10 mm/h. To recycle the crucibles and so to reduce the production costs, pBN crucibles were cleaned with hydrofluoric acid solution. As a result of this treatment, it was not possible to obtain $CrSi_2$ single crystals due to a modification of the crucible surface and the subsequent increase of boron compounds in the melt during the growth. The effect of the growth conditions on the microstructure of polycrystalline sample was also investigated using the texture analysis technique.

Keywords: A1. Directional solidification A2. Gradient freeze technique, A2. Single crystal growth, A2. Growth from melt B1. Silicide, B2. Semiconducting silicon compounds

1. Introduction

Semiconducting transition metal silicides have been largely developed these last decades providing new prospects on silicon-based microsystems integration [1, 2]. Among them, chromium disilicide ($CrSi_2$) has been largely studied as it possesses a high thermal stability up to 1000 K under air [3-7] and a small and indirect electronic bandgap (0.3 – 0.4 eV) [8-13]. This alloy can be considered for opto-electronic devices such as IR detectors [8, 14, 15], as thin film resistor [16, 17] and is particularly promising for thermoelectric applications [4, 13, 18-21].

$CrSi_2$ crystalizes in a C40 hexagonal structure with the $P6_222$ space group and lattice parameters a = 4.428 Å and c = 6.368 Å [4]. Large single crystals (up to 400 cm^3) have already been elaborated by the Czochralski method [11, 22-26] or by the zone melting method [12, 27-32]. Small single crystal

needles (up to 10 mm length and 0.3 mm diameter) have been obtained using tin flux with the Bridgman technique [3, 33-36] but it is not adapted for large crystal growth. To finish, centimetric manganese-doped $CrSi_2$ single crystals were grown by Shinoda *et al.* [11] using the Vertical Gradient Freeze (VGF) method without the use of a flux. However, the growth conditions and the quality of the crystals were not given in details. The VGF method is a variant of the Bridgman method which consist of moving the solid-liquid interface in a stationary crucible by lowering the temperature of the furnace instead of pulling down the crystal [37]. To our knowledge, no study of the growth mechanisms of $CrSi_2$ alloys with the VGF method were reported elsewhere.

To grow $CrSi_2$ crystals, the crucible has to be chemically compatible with Cr-Si to about 1800 K (maximum temperature which could be reached by the molten alloy) and its linear thermal expansion should be close to that of $CrSi_2$ in order to limit the thermo-mechanical stress and the dislocations. However, $CrSi_2$ has an anisotropic linear thermal expansion coefficient (LTEC) along *a* and *c* axis such as $\alpha_a = 24.10^{-6}$ K^{-1} and $\alpha_c = 10.10^{-6}$ K^{-1} at 1600 K [38] whereas for silica and pyrolytic boron nitride (pBN) crucible it is respectively about $0.5.10^{-6}$ K^{-1} (1000 K [39]) and 1.10^{-6} to 3.10^{-6} K^{-1} (300 K to 1273 K [40]). The difference of LTEC between $CrSi_2$ and the crucibles being more than one order of magnitude, it seems difficult to comply with this concern. Nevertheless, BN is material of choice for a crucible as it is known to be pretty stable with molten silicon and because molten silicon does not wet BN [41, 42]. This avoids sticking between the ingot and the crucible and limits the stress [43].

In this study we focus on the crystal growth of $CrSi_2$ ingots by the VGF method without the use of a flux nor the use of a seed to simplify the process. Two types of crucibles were investigated, SiO_2 crucibles with BN coating as they are pretty cheap for scaling up the process and pBN crucibles which are denser, to limit the contamination from the BN coating, but also more expensive. To decrease the cost, a pBN crucible was also recycled and cleaned with HF. The effect on the chemical composition and on the microstructure of the different ingots were investigated by texture analysis and the conditions to grow a $CrSi_2$ single crystal are given.

2. Material and methods

2.1. Materials elaboration

Stoichiometric amount of Cr granules (Alfa Aesar®, 99.99 %) and Si lumps (Alfa Aesar®, 99.9999 %) are melted together under Ar atmosphere (Air liquid®, 5N) by arc-melting. The apparatus is made of a tungsten electrode and a copper crucible both cooled with water. The obtained droplets are then crushed in an agate mortar in the shape of lump of less than 1 mm. 4 g are used to fill the silica glass crucible (SiO_2) with BN coating (spray coating from Final Advanced Materials® company) or to fill the pBN crucible (manufactured by Neyco® [40]). The typical dimensions are 40 mm and 80 mm in length with an inner diameter of 7 mm. The silica crucibles and pBN crucibles have respectively a flat and a conical bottom (about 30°) as shown in Figure 1-a and 1-b.

A schematic diagram of the vertical Bridgman growth furnace used in this experiment is shown in Figure 1-c. It is composed of a single conical shaped graphite heater specially designed to obtain a linear thermal gradient vertically and to minimize radial thermal gradients [44-46]. The crucible is maintained in the center of the heater using a graphite holder. The temperature gradient on the crucible is controlled by its vertical position in the heater. It is measured *in-situ* using two thermocouples placed at the top and at the bottom of the crucible (Figure 1-c). The accuracy of the thermocouples was estimated to be $\pm 3°C$ after calibration and their positioning could lead to additional experimental error as they are not in direct contact with the liquid.

In Figure 2-a is given an example of the measured top and bottom temperatures according to the crucible position in the furnace. A thermal gradient with a higher top temperature is obtained for a distance from the top of the heater more than 50 mm. Three purging in vacuum are performed at 300 K and at 573 K to eliminate potential released species, then the furnace is kept under static Ar atmosphere at 1.5 bar for the whole experiment (Air Product®, 5.2 N). The temperature is regulated with the bottom thermocouple (marked 4 on Figure 1-c). $CrSi_2$ alloy is melted by holding it at a temperature higher than 1750 K at the bottom of the crucible (which is above the melting point of 1712 K [47-49]), during 1 h. The cooling rate is first set to 5 - 10 K/h down to 1423 K to grow the crystal. It is increased to 50 K/h down to 1173 K and to 100 K/h down to 300K (See Figure 2-b). This two steps process was chosen to limit the thermal stress in the ingot.

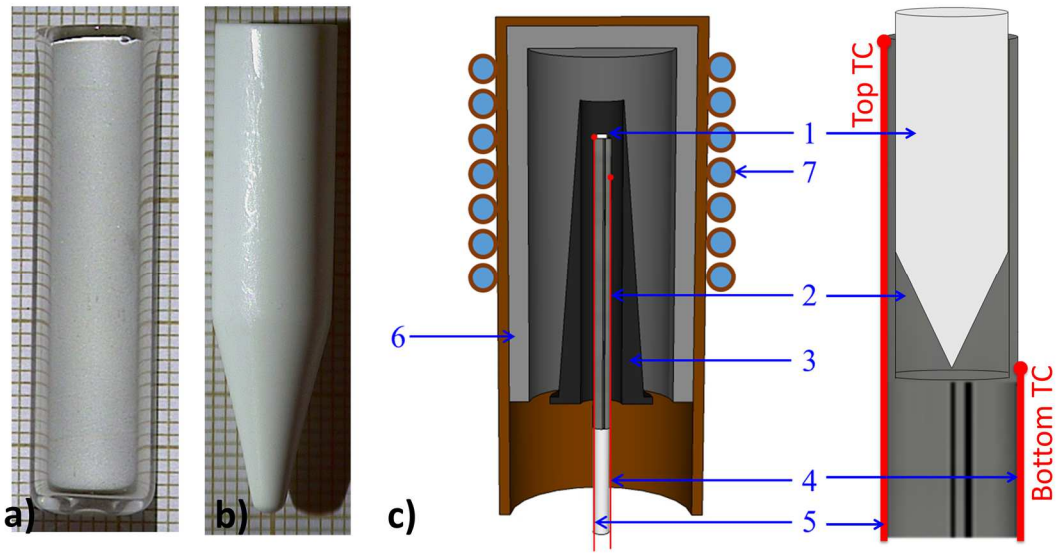

Figure 1: a) Silica glass crucible coated with BN b) pBN crucible c) schematic diagram of the VGF growth furnace (1- crucible; 2- graphite holder; 3- carbon heater; 4- bottom thermocouples; 5 – top thermocouple 6- carbon foam insulator; 7- water cooling).

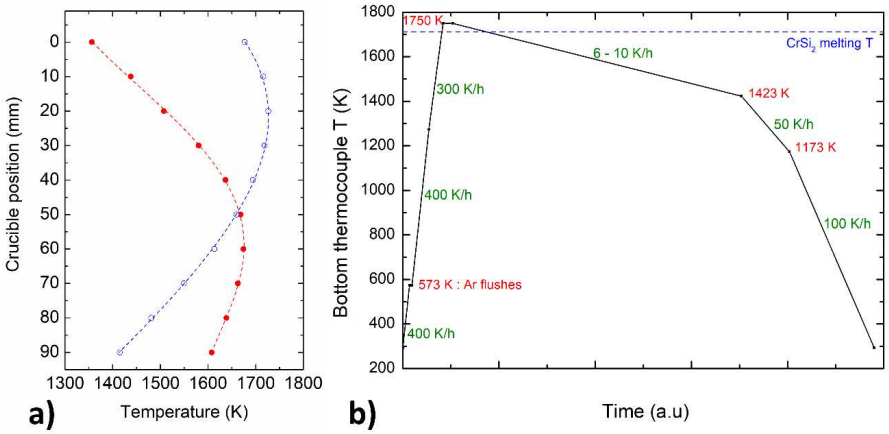

Figure 2: a) Temperature distribution in the furnace as a function of the position of the top of the 40 mm length crucible ○ Bottom thermocouple ● Top thermocouple (marked respectively 4 and 5 on Figure 1-c). The position 0 is taken as the top of the conical carbon heater. b) Temperature program controlled by the bottom thermocouple.

The experimental conditions are given in Table 1 for four selected ingots. The ingot (A) is elaborated in silica glass crucible with BN coating. The ingots (B), (C) and (D) are elaborated in pBN crucibles. The crucible of the ingot (C) was previously treated with hydrofluoric acid (HF). Ingots (B) and (C) are obtained with similar conditions and ingot (D), which is longer to consider scaling-up, is obtained at higher growth rate. The maximum temperature reached by ingot (A) is about 1820 K. For ingots (B) and (C) it is about 1775K whereas it is about 1800 K for the ingot (D) as it is longer.

Ingot	Crucible type	Cooling rate (K/h)	Thermal gradient (K/mm)	Growth rate (mm/h)
(A)	*40 mm Length* SiO_2 + BN coating	10	1.7	6
(B)	*40 mm Length* pBN	6	0.6	10.0
(C)	*40 mm Length* HF treated pBN	6	0.6	10.0
(D)	*80 mm Length* pBN	10	0.6	22

Table 1: Experimental growth conditions (cooling rate, thermal gradient and growth rate) of 4 ingots grown in 40 and 80 mm length, 7 mm inner diameter crucible in (A) Silica glass (SiO_2) coated with BN, (B) and (D) pBN, (C) pBN treated with HF.

2.2. Characterization

The droplets obtained after arc melting and the ingots obtained by VGF were analyzed using a powder X-Ray Diffraction apparatus (Philips X'PERT, Cu-Kα radiation 1.5406 Å with an accelerated detector PW3050/60 at 45 kV and 30mA settings). The droplets were only composed of the $CrSi_2$ phase and every droplet containing a secondary phase was removed at this step (diffraction pattern is given in S.I. Fig. S1). The chemical homogeneity and the composition of the ingot (A) were checked using an SDD Oxford Instrument X-Max 50 mm^2 Energy Dispersive X-Ray Spectroscopy (EDX) detector mounted on a FEI Quanta 200 FEG Scanning Electron Microscope (SEM). The chemical composition of the single crystalline ingot (B) was measured using an electron probe micro analysis on a CAMECA SX-100 instrument equipped with five wavelength-dispersive X-ray spectrometers (WDS) at the Service Microsonde Sud (Montpellier). Electron Back Scattering Diffraction (EBSD) analysis were carried out on ingot (B), (C) and (D) with a CamScan Crystal Probe X500FE SEM equipped with an EDX X-MaxN 20 mm^2 detector and HKL NordlysNano EBSD detector. The data were acquired with step sizes from 5 to 15 µm depending on the crystalline size to probe and treated with CHANNEL5 (Oxford Instrument) software. Polycrystalline ingots (C) and (D) were characterized by texture analysis in terms of misorientation angle distribution, pole figures and population categories [50]. The population categories can be separated as: the "correlated" plot which displays the misorientation distribution between two adjacent grains; the "uncorrelated" population which displays the misorientation between random pairs from the grain list. The latter enables to determine the misorientation angle distribution considering no interaction between grains. For ingots (C) and (D), respectively 3319 and 1442 pairs of correlated grains were considered, and 5000 random pairs in both cases. The increase of the random pair population doesn't change the statistics. These two statistics were compared with a random distribution given by the Mackenzie plot in the case of an hexagonal space group [51, 52]. The misorientation angles below 5° are removed to avoid the mosaicity effect and to limit instrumental errors [53].

Laue neutron diffraction patterns were recorded in back-reflection geometry on ingot (B) on the Orient-Express diffractometer at the Institute Laue Langevin (ILL) using two high-performance image-intensified CCD cameras coupled to a large-area neutron scintillator [54]. The stationary crystal was irradiated 1 min with a polychromatic neutron beam from 0.8 to 3.2 Å. Data were treated with Cologne Laue Indexation Program (CLIP) [55].

3. Results and Discussion

The good melting of the starting materials was observed *ex-situ* by looking at the overall homogeneity of the ingots and at their shape which were found to be similar to that of the crucibles (See Figure 3). The crystal growth conditions of ingot (A), grown in silica crucible with BN coating, will be first discussed followed by a discussion on ingots (B), (D) and (C), grown in new and in recycled pBN

crucible using HF treatment. The first difference we observe is the difference of the bottom shape of the ingot (C) compared to the ingots (B) and (D). This difference could be attributed to a modification of the interface between the crucible and the molten $CrSi_2$. One possible explanation would be that the wettability of $CrSi_2$ increases due to the formation of NH_4BF_4 at the interface by a reaction between HF and BN [56, 57]. Nevertheless, this assumption needs further investigation to confirm. To notice, a low wettability between the crucible and the melt is interesting to limit heterogeneous nucleation on the walls and to reduce the interactions between the molten elements and the crucible. The impact of the crucible and of the growth conditions on the microstructure are discussed in detail in the following paragraphs.

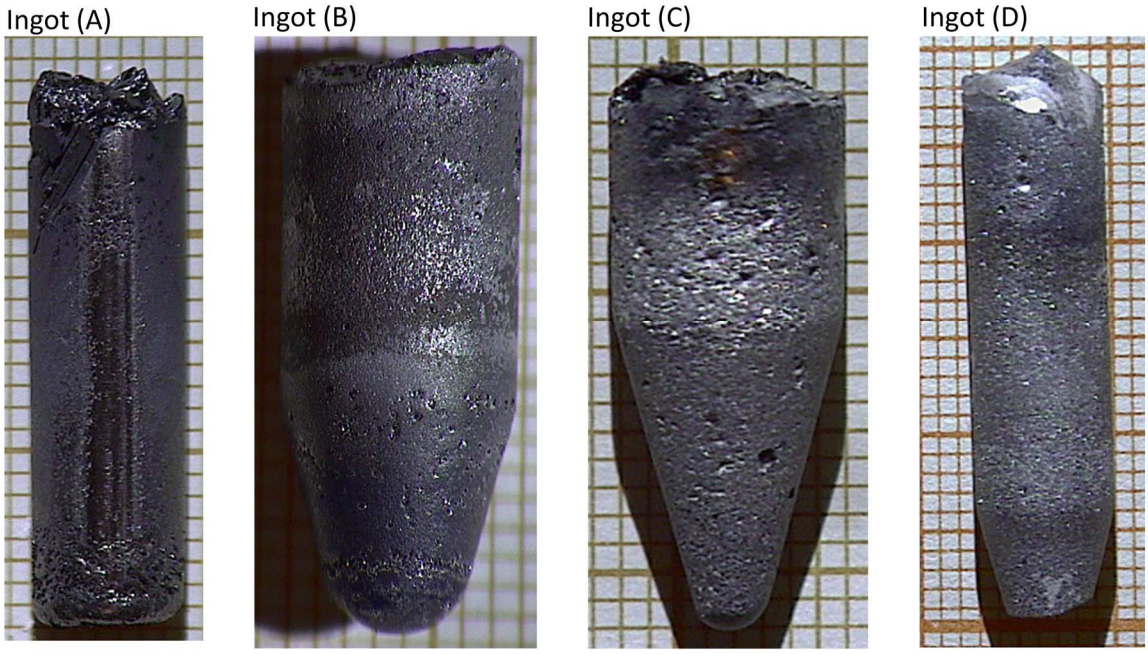

Figure 3: Optical image of ingot (A) to (D).

3.1. Crystal growth in silica glass crucible with BN coating

The SEM back-scattered images of the ingot (A) are given in the Figure 4 after polishing the surface. Two main phases are observed along the ingot, a light grey phase which covers most of the surface and a black phase with irregular faceted shapes (from 100 to 200 µm length) only at the bottom and at the top of the ingot. The chemical composition of the areas marked from 1 to 5, are given in Table 2. It shows that the areas 1, 4 and 5 with light grey contrast corresponds to the $CrSi_2$ phase with an atomic ratio close to the theoretical value of 2. These results also show that the $CrSi_2$ composition is the same all along the ingot. One can also observe that the oxygen content is negligible (below 2 at.%) and that the black areas possess a high content of carbon and silicon (areas 2 and 3). We do not observe at this resolution B- or N-rich phases. The large amount of carbon found in areas 1, 4 and 5 comes from external contamination and residual carbon in the SEM vacuum chamber. Indeed, the carbon solubility limit in $CrSi_2$ is expected to be low or even negligible [58].

From our powder XRD characterization of the volume of the top and of the center of the ingot, (see Figure 5), one observes the presence of $CrSi_2$ as the main phase and of minor secondary phases such as SiC, CrB and Cr_5Si_3. There is consequently a contamination of the Cr-Si alloys by C and B coming respectively from the furnace (most of the components are made of C graphite) and from the BN coating of the crucible. This carbon contamination is also observed for silicon crystal growth and can be explained by a reaction between the silica crucible and the carbon holder [59-63]. A tentative explanation of the presence of SiC can be given following the behavior already observed on silicon crystal [59, 63].

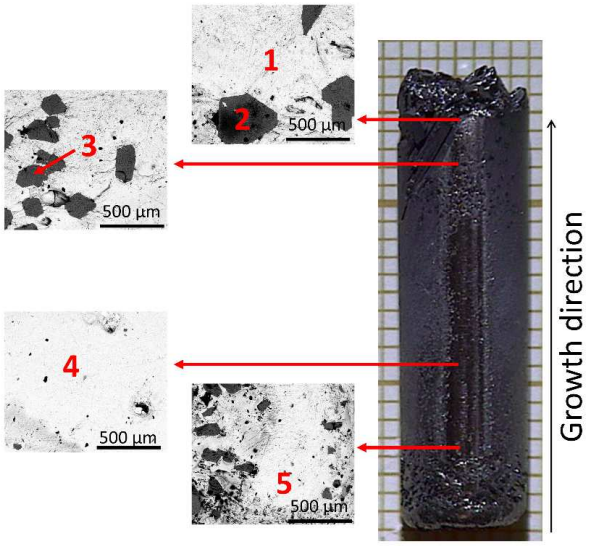

Figure 4: Optical image of the ingot (A) elaborated in silica glass crucible (right) and backscattered SEM images near the surface of the ingot at different positions (left). The different areas analyzed by EDX are identified from 1 to 5.

Composition (%at.)	1	2	3	4	5
Si	57,2	48,2	35,3	57,1	57,4
Cr	31,4	0,0	0,4	30,5	31,6
C	11,4	53,6	62,4	12,4	10,6
O	0,0	1,2	2,0	0,0	0,4
Si/Cr	1,8	/	/	1,9	1,8

Table 2: Chemical composition of Si, Cr, C and O near the surface of the ingot given by EDX from the five areas, noted 1 to 5 and identified in Figure 4. The Si/Cr ratio is also given in the homogeneous areas.

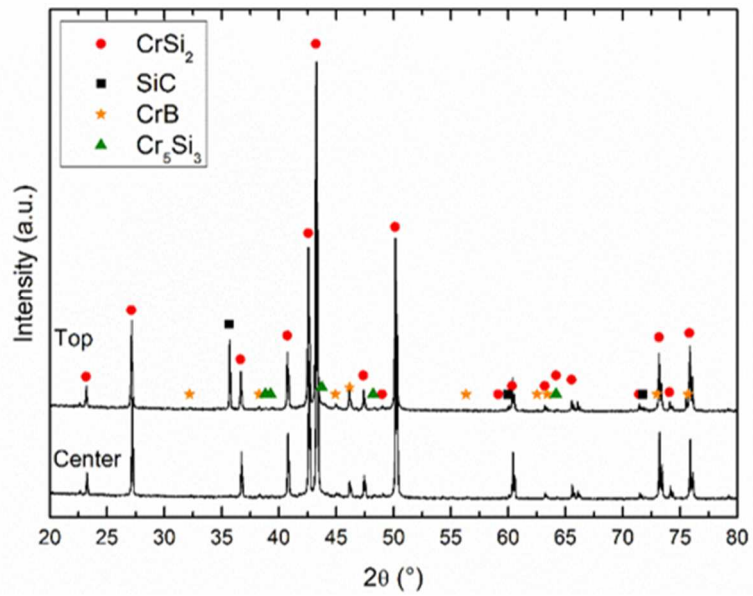

Figure 5. Powder X-Ray Diffraction of ingot (A) at the center and at the top of the ingot. Secondary phases are observed and indexed on the top pattern. The phase indexation is made from the ICDD PDF database ($CrSi_2$: 04-016-2861, SiC: 04-008-2393, CrB: 01-089-3587, Cr_5Si_3: 04-001-7859).

The maximum temperature reached by the crucible ranges from 1750 K (bottom) and 1820 K (top). The reactions which can occur are listed below:

$$3C_{(s)} + SiO_{2\,(s)} \longrightarrow SiC_{(s)} + 2CO_{(g)} \qquad (1)$$

$$C_{(s)} + SiO_{2\,(s)} \rightarrow SiO_{(g)} + CO_{(g)} \qquad (2)$$

With the reaction (1) and (2) one observes the formation of $SiC_{(s)}$, $SiO_{(g)}$ and $CO_{(g)}$ at the interface between the crucible and the graphite holder. The $SiO_{(g)}$ should condense in the colder parts of the furnace and this is what we observe in the shape of needle of less than 1mm. Concerning the carbon monoxide, $CO_{(g)}$, it can dissolve in the molten $CrSi_2$ following the reaction (3) such as:

$$CrSi_{2\,(l)} + 0{,}7CO_{(g)} \longrightarrow 0{,}7SiC_{(s)} + 0{,}7SiO_{(g)} + 0{,}2Cr_5Si_{3\,(s)} \qquad (3)$$

Through this reaction, SiC and Cr_5Si_3 should be obtained in the melt. This is indeed what was observed by XRD (see Figure 5). As described previously, the presence of SiO is also observed in the cold areas of the furnace. The presence of SiC at the bottom and at the top of the crucible could be explained by segregation mechanisms widely presented in the literature during Si crystal growth [64, 65]. To notice, as silica crucibles are well adapted for large scale development of the process, and are already used in the industry because of their low price and easy manufacture, it would be suitable to use a furnace without graphite elements. However, the BN coating between the silica crucible and the melt has to be optimized and densified in order to limit the heterogeneous nucleation on the wall or on

small BN particles which could come off. Another solution would be to use pyrolytic BN crucible to avoid carbon contamination and this will be discussed in the next section.

3.2. Crystal growth in pBN crucible

The EBSD band contrast images with secondary phases coloration of the ingots (B), (C) and (D) are given in Figure 6. As expected, we do not observe the presence of SiC with the use of pBN crucible, confirming its origin from the reaction between SiO_2 and C. Nevertheless, small amounts of chromium borides (CrB, CrB_2 and Cr_3B_4) (below 5 w.%) were identified in both ingots and come from the reaction with the boron of the crucible. One also notices several pores surrounded by small Cr_5Si_3 precipitates which may have appeared after tearing off larger Cr_5Si_3 precipitates while dicing and polishing the ingot. It is not surprising to observe that borides precipitates are more important in the ingot (C) than in the ingot (B) and (D) as HF treatment could have modified the surface of the crucible in terms of chemical composition, wettability and roughness. One also notices that the amount of secondary phases is also important at the bottom of the ingot (D) despite of the use of a new crucible. As described previously, this ingot is subjected to a higher temperature (about 1800 K *vs* 1775 K) which could increase the reaction/diffusion of boron with/in the Cr-Si melt. The presence of large boron amount leads to the consumption of chromium and the subsequent rejection of silicon at the top of the ingot.

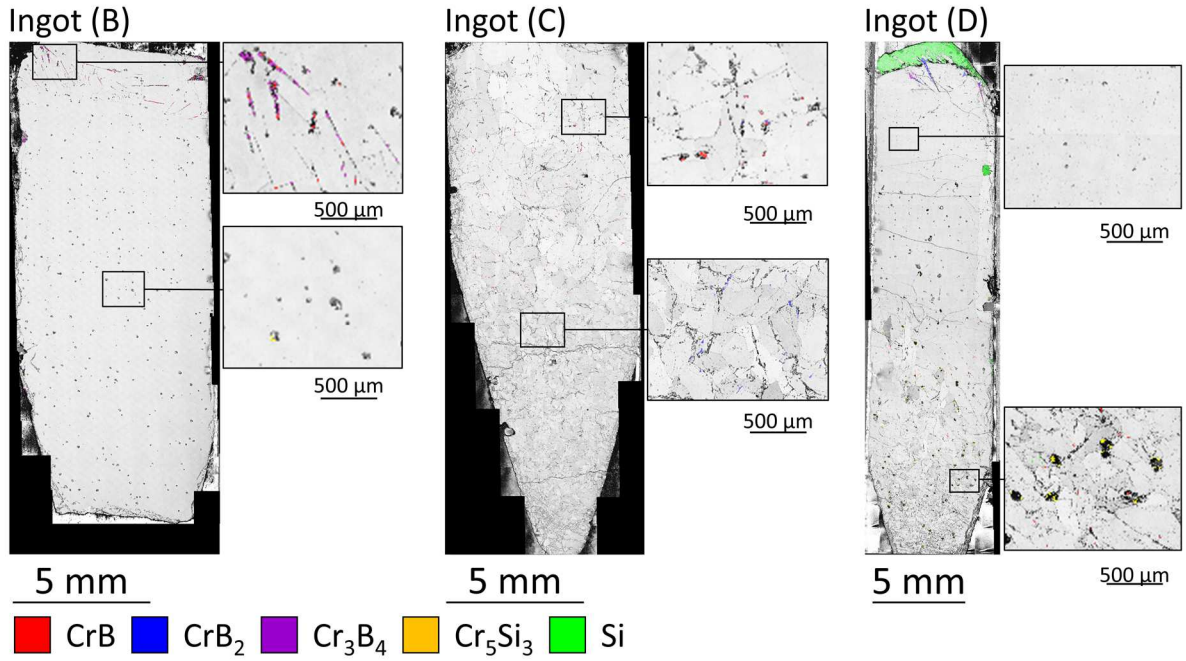

Figure 6: Optical and EBSD band contrast (cross-section) images of the ingots (B) and (C). The secondary phases identified by EBSD are colored. The grey parts are indexed to $CrSi_2$.

The EBSD orientation maps and the pole figures of the ingots (B), (C) and (D) are given in Figure 7. One observes that the ingot (B) is about 95% monocrystalline with a growth direction along the $<01\bar{1}0>$ axis. The quality of this single crystal is confirmed in Figure 8-a, showing the amplified texture map of the ingot with a misorientation angle ranging from 0° to 5°. The top and the edges of the ingot have a misorientation angle higher than 1° and the center of the ingot has a misorientation angle below 0.5°. The Laue neutron diffraction pattern is given in Figure 8-b to probe the entire volume of the ingot. Every spot can be indexed with the $CrSi_2$ phase with the zone axis near <0001> confirming the single crystalline state of the ingot. A mosaicity of about 1 to 2° can be estimated according to the spot length. The chemical composition of the ingot (B) was characterized by WDS. It is homogeneous all along the ingot and shows a small silicon deficit in the material corresponding to the stoichiometry $CrSi_{1.96}$. This result is consistent with the existing domain of $CrSi_2$ given in the literature [22, 66, 67].

Concerning the ingots (C) and (D), they are made of numerous columnar and equiaxed grains with increasing size during the growth. The rough shape of the grains observed in both ingots can be explained by the well-known Jackson's factor [68] such as:

$$\alpha = \frac{\eta}{Z}\frac{L}{k_B T_m}$$

where η is the number of nearest neighbor sites adjacent to an atom in the plane of the interface, Z, the total number of nearest neighbors of an atom in the crystal, L, the latent heat of fusion, k_B, the Boltzmann constant and T_m, the melting point of the alloy. If $\alpha > 2$, a faceted interface can be expected whereas if $\alpha < 2$ a rough interface is obtained. In general, metals usually have $\alpha < 2$ whereas for semiconductors $2 < \alpha < 3$. For $CrSi_2$ using $Z = 10$, $L = 42.1$ kJ.mol^{-1} [69] and $T_m = 1712$ K, one obtains $\alpha = 0.59$ in the (0001) plan and $\alpha = 1.48$ in the $(01\bar{1}0)$ plan. These results are consistent with the morphology observed in ingots (C) and (D) where a rough interface is observed. It is interesting to notice that the values of α obtained for $CrSi_2$ are lower than those of semiconductors [70, 71] which means that $CrSi_2$ has a growth behavior close to the one of metallic compounds.

From the orientation maps and the pole figures given in Figure 7 one observes that the grains of the ingots (C) and (D), in contact with the crucible, have a preferential orientation which is predominant throughout the ingot. Ingot (C) has a preferential growth direction along $< 01\bar{1}0 >$ axis, as for ingot (B), whereas for ingot (D), elaborated with a higher crystal growth rate, it is slightly shifted to this axis. This shift has already been described when the crystal growth rate in silicon is increased [72]. To notice, for $CrSi_2$ nanowires or needles growth (with the use of a flux), the preferential growth direction is along the $< 0001 >$ axis [3, 73, 74]. As the nanowires and the needles are free to grow in each direction, this means that the $< 0001 >$ axis would have the highest growth kinetic. Indeed, this kinetic

direction extends at high growth rate or without other competing grains. At low growth rate and without the use of a flux, this kinetic growth direction competes with other orientations and the grain direction with lower surface energy extends to the lateral direction [75-77]. This could explain why we found a $< 01\bar{1}0 >$ preferential growth direction for our ingots.

Concerning the equiaxed microstructure, it could be explained by the presence of Cr-B precipitates in the ingots (C) and (D) as they could have act as seeds for the nucleation and the growth of these equiaxed grains. One also notices in ingot (D) that the amount of precipitates decreases all along the ingot as well as the amount of grains. To have a better insight of the interaction between the grains, a texture analysis is given in Figure 9. The misorientation angle distribution, the pole figure and the population categories compared to the Mackenzie distribution are given for these two ingots.

In the case of the ingot (C), a good agreement between correlated and uncorrelated populations is observed for angles higher than 10° showing that the microstructure for these grains is not due to physical interactions between them. Nevertheless, the growth is not completely random as a large difference between the experimental distributions (either correlated or uncorrelated) and the Mackenzie plot is observed for all misorientation angles. A maximum of experimental misorientation is found around 30° whereas it should be around 90° for random hexagonal materials. It has been reported in the literature that this effect can reveal a preferential orientation along the *c*-axis [78, 79]. This behavior is confirmed by the pole figure where the *c*-axis is preferentially observed perpendicular to the growth as observed in the entire ingot in Figure 7. Below 10°, the number of correlated grains is more important than the uncorrelated ones. This effect is characteristic of the presence of subgrains obtained by inheritance effect [80].

In the case of the ingot (D), grown at higher growth rate, the experimental misorientation populations are similar with the Mackenzie distribution for angles higher than 20°. It means that the grains misoriented with more than 20° are randomly formed, as confirmed by the pole figure. Nevertheless, a minor population with preferential orientation is observed for misorientation angles below 20° whereas it is about 30° for ingot (C). To finish, the peak below 10° is also explained by a large subgrain formation. Therefore, a random and a textured grain population are encountered in the polycrystalline part of this ingot. The important random part can be due to the high growth rate applied during the growth of this ingot. Based on these results, an increase of the growth rate could favor an inclination of the growth direction and a random grain orientation of the equiaxed grains.

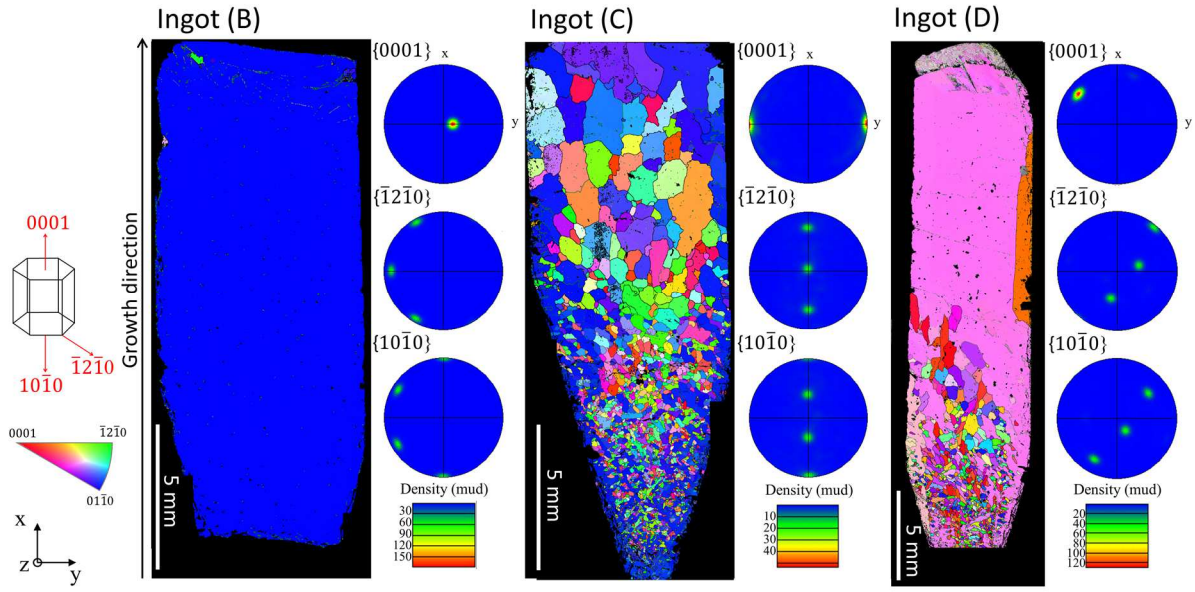

Figure 7: x direction Inverse Pole Figure (IPF) color maps and pole figure of the ingots (B), (C) and (D). The grain boundaries are indicated in black lines for misorientation above 10° and green lines for misorientation between 2° and 10° (subgrains).

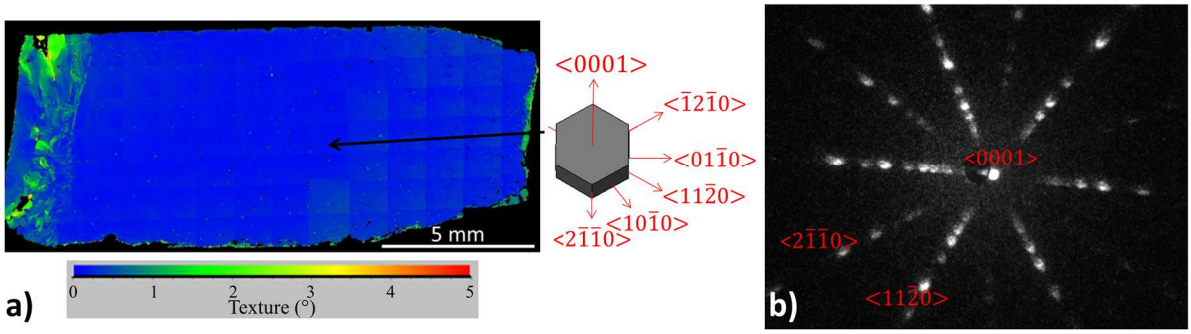

Figure 8: a) Texture analysis by EBSD and b) neutron Laue diffraction pattern of the ingot (B).

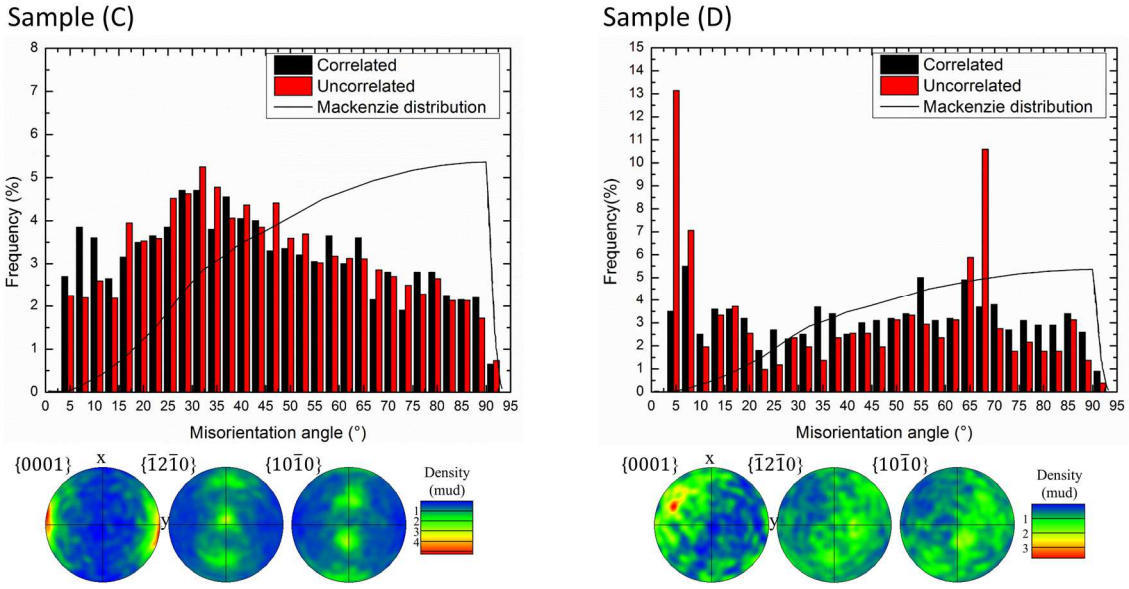

Figure 9: Misorientation angle distribution and pole figure for correlated and uncorrelated grains of the ingots (C) (left) and (D) (right) compared to the Mackenzie distribution (x and y axis of Figure 7).

4. Conclusion

Single and polycrystalline chromium disilicide ingots were grown with the Vertical Gradient Freeze method in BN-coated silica and pBN crucibles with a conical shape about 30°. Although silica crucibles would be more convenient for scaling up the process, their use still needs further investigation. Indeed, a reaction between the SiO_2 crucible and the carbon graphite from the furnace leads to the formation of SiC in the melt. We also show that the use of pBN crucibles enables to avoid such contamination. In order to reduce the costs of the manufacturing process, a pBN crucible was recycled and cleaned with HF. However, the HF cleaning shows that HF modifies the interaction between the melt and the crucible, probably because of chemical alteration of the crucible surface, and so modification of the wettability and the roughness.

Nevertheless, this investigation shows that it is possible to grow $CrSi_2$ single crystal with a low mosaicity (less than 2°) in new pBN crucible with a growth rate of 10 mm/h and a thermal gradient of 0.6 K/mm. The preferential growth direction for the three ingots grown in pBN crucible is along $< 01\bar{1}0 >$ axis or with a slight shift to this direction. As observed experimentally, it was shown with the Jackson's factor that the interface is rough. Also and as expected, when the amount of impurities increases, the amount of columnar and equiaxed grains increases. One also shows that a higher growth rate (22mm/h) leads to an inclination of the columnar grains and favor the random grain orientation. To notice, under this growth rate one observes a transition from an equiaxed microstructure to a single crystal. This could be explained by the decrease of the impurities along the ingot and would be

promising for large-scale application but deserves further investigations to optimize the microstructure.

Acknowledgments

The authors would like to thank T. Duffar and F. Mercier (SIMaP Grenoble) for respectively providing us the oven and for fruitful discussion on the upgrade of the oven to high temperature, A. Vieira e silva (ICG Montpellier) for its technical support, C. Nevado (Géosciences Montpellier) for the ingot preparation for EBSD analysis and B. Boyer (Géosciences Montpellier) for WDS analysis. We also want to thank M. Boehm and the Institut Laue-Langevin (ILL, Grenoble) for the characterization on the Laue diffractometer OrientExpress.

References

[1] H. Lange, Electronic Properties of Semiconducting Silicides, Physica status solidi (b), 201 (1997) 3-65.
[2] V.E. Borisenko, Semiconducting Silicides, Springer, Berlin, Heidelberg, 2000, pp. 239-241.
[3] T. Shishido, S. Okada, Y. Ishizawa, K. Kudou, K. Iizumi, Y. Sawada, H. Horiuchi, K. Inaba, T. Sekiguchi, J. Ye, S. Miyashita, A. Nomura, T. Sugawara, K. Obara, M. Oku, K. Fujiwara, T. Ujihara, G. Sazaki, N. Usami, S. Kohiki, Y. Kawazoe, K. Nakajima, Molten metal flux growth and properties of $CrSi_2$, Journal of Alloys and Compounds, 383 (2004) 319-321.
[4] T. Dasgupta, J. Etourneau, B. Chevalier, S.F. Matar, A.M. Umarji, Structural, thermal, and electrical properties of $CrSi_2$, Journal of Applied Physics, 103 (2008) 113516.
[5] J. Ma, Y. Gu, L. Shi, L. Chen, Z. Yang, Y. Qian, Synthesis and thermal stability of nanocrystalline chromium disilicide, Journal of Alloys and Compounds, 376 (2004) 176-179.
[6] J. Lu, H. Yang, B. Liu, J. Han, G. Zou, Preparation and physical properties of nanosized semiconducting $CrSi_2$ powders, Materials Chemistry and Physics, 59 (1999) 101-106.
[7] D. Stathokostopoulos, D. Chaliampalias, E. Tarani, A. Theodorakakos, V. Giannoulatou, G.S. Polymeris, E. Pavlidou, K. Chrissafis, E. Hatzikraniotis, K.M. Paraskevopoulos, G. Vourlias, Formation of the Thermoelectric Candidate Chromium Silicide by Use of a Pack-Cementation Process, Journal of Electronic Materials, 43 (2014) 3733-3739.
[8] M.C. Bost, J.E. Mahan, An investigation of the optical constants and band gap of chromium disilicide, Journal of Applied Physics, 63 (1988) 839-844.
[9] A.V. Krivosheeva, V.L. Shaposhnikov, V.E. Borisenko, Electronic structure of stressed $CrSi_2$, Materials Science and Engineering: B, 101 (2003) 309-312.
[10] L.F. Mattheiss, Electronic structure of $CrSi_2$ and related refractory disilicides, Physical Review B, 43 (1991) 12549-12555.
[11] D. Shinoda, S. Asanabe, Y. Sasaki, Semiconducting properties of chromium silicides, Journal of the Physical Society of Japan, 19 (1964) 269-272.
[12] I. Nishida, The crystal growth and thermoelectric properties of chromium disilicide, Journal of Materials Science, 7 (1972) 1119-1124.
[13] I. Nishida, T. Sakata, Semiconducting properties of Pure and Mn-doped chromium disilicide, Journal of Physics and Chemistry of Solids, 39 (1978) 499-505.
[14] D. Goroshko, E. Chusovitin, A. Shevlyagin, M. Bozhenko, R. Batalov, R. Bayazitov, N. Galkin, Enhancement of near IR sensitivity of silicon-silicide based photodetectors, physica status solidi (c), 10 (2013) 1844-1846.
[15] D.B. Migas, V.E. Borisenko, Semiconducting silicides as potential candidates for light detectors:ab initio predictions, physica status solidi (c), 10 (2013) 1658-1660.

[16] K. Hieber, R. Dittmann, Structural and Electrical Properties of $CrSi_2$ Thin Film Resistors, Thin Solid Films, 36 (1976) 357-360.
[17] X. Dong, J. Wu, Formation of an intermetallic phase by crystallization in the Cr–Si–Ni–Al amorphous film, Journal of Alloys and Compounds, 359 (2003) 256-260.
[18] B.K. Voronov, L.D. Dudkin, N.N. Trusova, The features of physical chemical structure of chromium disilicide (in Russian), in: Khimicheskaya Svyaz v Poluprovodnikah, Nauka i Tekhnika, Minsk, 1969, pp. 291.
[19] D.M. Rowe, Thermoelectrics Handbook - Macro to Nano, in, Taylor & Francis Group, LLC, 2006, Chap. 31-31 - 31-33.
[20] S. Karuppaiah, M. Beaudhuin, R. Viennois, Investigation on the thermoelectric properties of nanostructured $Cr_{1-x}Ti_xSi_2$, Journal of Solid State Chemistry, 199 (2013) 90-95.
[21] M. Khalil, M. Beaudhuin, B. Villeroy, D. Ravot, R. Viennois, A modeling approach for new $CrSi_2$ based alloys: Application to metastable $Cr_{1-x}Zr_xSi_2$ as a potential thermoelectric material, Journal of Alloys and Compounds, 662 (2016) 150-156.
[22] B.K. Voronov, L.D. Dudkin, N.I. Kiryukhina, N.N. Trusova, A physicochemical Study of a Chromium Disilicide-Based Phase, Izvestiya Akademii Nauk SSSR, Neorganicheskie Materialy, 4 (1968) 325-330.
[23] B.K. Voromov, L.D. Dudkin, N.I. Kiryuchina, N.N. Trusova, Investigation of the Cr-Si system in the disilicide region, Soviet Powder Metallurgy and Metals Ceramics, 6 (1967) 56-61.
[24] V.I. Kaidanov, V.A. Tselishchev, A.P. Usov, L.D. Dudkin, B.K. Voronov, N.N. Trusova, Anisotropy of the Transport Properties of Chromium Disilicide, Soviet Physics - Semiconductors, 4 (1971) 1135-1141.
[25] O. Chaix-Pluchery, G. Lucazeau, Vibrational Study of Transition Metal Disilicides, MSi_2 (M = Nb, Ta, V, Cr), Journal of Raman Spectroscopy, 29 (1998) 159-164.
[26] J.C. Lasjaunias, U. Gottlieb, O. Laborde, O. Thomas, R. Madar, Transport and Low Temperature Specific Heat Measurements of $CrSi_2$ Single Crystals, MRS Proceedings, 402 (1996) 343-348.
[27] K. Tanaka, K. Nawata, H. Inui, M. Yamaguchi, M. Koiwa, Refinement of crystallographic parameters in transition metal disilicides with the C11b, C40 and C54 structures, Intermetallics, 9 (2001) 603-607.
[28] I.J. Ohsugi, T. Kojima, I.A. Nishida, Temperature dependence of the magnetic susceptibility of a $CrSi_2$ single crystal, Physical Review B, 42 (1990) 10761-10764.
[29] Z.J. Pan, L.T. Zhang, J.S. Wu, Effects of Al doping on the transport performances of $CrSi_2$ single crystals, Scripta Materialia, 56 (2007) 245-248.
[30] Z.J. Pan, L.T. Zhang, J.S. Wu, Effects of V doping on the transport performances of $CrSi_2$ single crystals, Scripta Materialia, 56 (2007) 257-260.
[31] T. Hirano, M. Kaise, Electrical resistivities of single-crystalline transition-metal disilicides, Journal of Applied Physics, 68 (1990) 627-633.
[32] M. Nakamura, Elastic Constants of Some Transition-MetaI-Disilicide Single Crystals, Metallurgical and Materials Transactions A, 25 (1994) 331-340.
[33] P. Peshev, M. Khristov, G. Gyurov, The growth of titanium, chromium and molybdenum disilicide crystals from high-temperature solutions, Journal of the Less Common Metals, 153 (1989) 15-22.
[34] T. Shishido, S. Okada, Y. Ishizawa, K. Kudou, K. Iizumi, Y. Sawada, H. Horiuchi, K. Inaba, T. Sekiguchi, J. Ye, S. Miyashita, A. Nomura, T. Sugawara, K. Obara, Y. Murakami, K. Fujiwara, T. Ujihara, G. Sazaki, N. Usami, M. Oku, Y. Yokoyama, S. Kohiki, Y. Kawazoe, K. Nakajima, High-Temperature Solution Growth and Characterization of Chromium Disilicide, Japanese Journal of Applied Physics, 42 (2003) 7292-7293.
[35] F.Y. Solomkin, V.K. Zaitsev, N.F. Kartenko, A.S. Kolosova, A.T. Burkov, O.N. Uryupin, A.A. Shabaldin, Structure and thermoelectric properties of $CrSi_2$ crystallized from a tin solution—melt, Technical Physics, 55 (2010) 750-752.
[36] F.Y. Solomkin, V.K. Zaitsev, N.F. Kartenko, A.S. Kolosova, A.S. Orekhov, A.Y. Samunin, G.N. Isachenko, Crystallization and properties of $CrSi_2$ single crystals grown from a tin solution-melt, Technical Physics, 55 (2010) 151-153.

[37] P. Rudolph, Handbook of Crystal Growth: Bulk Crystal Growth: Basic Techniques, in, 2015, Chap. 9.
[38] I. Engström, B. Lönnberg, Thermal expansion studies of the group IV-VII transition-metal disilicides, Journal of Applied Physics, 63 (1988) 4476.
[39] N.P. Bansal, R.H. Doremus, Handbook of Glass Properties, Elsevier, Chap.6, 2013.
[40] Neyco, Refractory ceramics, https://www.neyco.fr/en/our-products/materials/refractory-materials/refractory-ceramics, Retrieved November 2019
[41] C. Huguet, C. Dechamp, R. Voytovych, B. Drevet, D. Camel, N. Eustathopoulos, Initial stages of silicon–crucible interactions in crystallisation of solar grade silicon: Kinetics of coating infiltration, Acta Materialia, 76 (2014) 151-167.
[42] W. Polkowski, N. Sobczak, R. Nowak, A. Kudyba, G. Bruzda, A. Polkowska, M. Homa, P. Turalska, M. Tangstad, J. Safarian, E. Moosavi-Khoonsari, A. Datas, Wetting Behavior and Reactivity of Molten Silicon with h-BN Substrate at Ultrahigh Temperatures up to 1750 °C, Journal of Materials Engineering and Performance, 27 (2017) 5040-5053.
[43] P. Rudolph, Handbook of Crystal Growth: Bulk Crystal Growth: Basic Techniques, in, 2015, pp. 349.
[44] A. Rouzaud, Influence des convections thermique et thermosolutale sur les ségrégations observées lors de la croissance cristalline d'alliages Ge-Si et Ge-Ga, Thèse de Doctorat, Grenoble, (1984).
[45] D. Camel, J.J. Favier, A. Rouzaud, Four de cristallogenèse, Brevet Brevatome, n°8411386, (1986).
[46] B. Angelier, Apport de la simulation numérique à la définition de la thermique d'un four spatial de cristallogenèse in, CNAM, Grenoble, Thèse de doctorat, 1994.
[47] Y. Chang, Phase Relationships in the System Chromium-Silicon, Transactions of The Metallurgical Society of AIME, 242 (1968) 1509-1515.
[48] Y. Du, J.C. Schuster, Experimental reinvestigation of the CrSi-Si partial system and update of the thermodynamic description of the entire Cr-Si system, Journal of Phase Equilibria, 21 (1999) 281-286.
[49] H. Okamoto, Cr-Si (Chromium-Silicon). , Journal of Phase Equilibria and Diffusion, 22 (2001) 593.
[50] V. Randle, O. Engler, Introduction to Texture Analysis: Macrotexture, Microtexture and Orientation Mapping, in, CRC Press 2014, pp. 283.
[51] J.K. Mackenzie, M.J. Thomson, Some statistics associated with the random disorientation of cubes, Biometrika, 44 (1957) 205-210.
[52] J.K. Mackenzie, Second paper on statistics associated with the random disorientation of cubes, Biometrika, 45 (1958) 229-240.
[53] D. Prior, Problems in determining the misorientation axes, for small angular misorientations, using electron backscatter diffraction in the SEM, Journal of Microscopy, 195 (1999) 217-225.
[54] B. Ouladdiaf, J. Archer, G.J. McIntyre, A.W. Hewat, D. Brau, S. York, OrientExpress: A new system for Laue neutron diffraction, Physica B: Condensed Matter, 385-386 (2006) 1052-1054.
[55] O.J. Schumann, Cologne Laue Indexation Program, http://clip4.sourceforge.net/, Retrieved 29/08/2018
[56] K. Niedenzu, J.W. Dawson, Boron Nitride, in: Boron-nitrogen compounds, Springer Science & Business Media, 1965.
[57] I.Y. Kelina, N.I. Ershova, Y.A. Drobinskaya, L.A. Plyasunkova, Chemical stability of a composite material based on silicon and boron nitrides, Refractories and industrial ceramics, 39 (1998) 404-410.
[58] Y. Du, J.C. Schuster, Experimental Investigation and Thermodynamic Description of the Constitution of the Ternary System Cr-Si-C, Journal of American Ceramic Society, 83 (2000) 2067-2073.
[59] F. Schmid, C.P. Khattak, T.G. Digges, L. Kaufman, Origin of SiC Impurities in Silicon Crystals Grown from the Melt in Vacuum, Journal of the Electrochemical Society, 126 (1979) 935-938.
[60] H.M. Liaw, Oxygen and carbon in Czochralski-grown silicon, Microelectronics Journal, 12 (1981) 33-36.
[61] X. Liu, B. Gao, K. Kakimoto, Numerical investigation of carbon contamination during the melting process of Czochralski silicon crystal growth, Journal of Crystal Growth, 417 (2015) 58-64.

[62] X. Liu, B. Gao, S. Nakano, K. Kakimoto, Reduction of carbon contamination during the melting process of Czochralski silicon crystal growth, Journal of Crystal Growth, 474 (2017) 3-7.
[63] P. Rudolph, Handbook of Crystal Growth: Bulk Crystal Growth: Basic Techniques, in, 2015, Chap. 10.13.15.
[64] M. Beaudhuin, T. Duffar, M. Lemiti, K. Zaidat, One-dimensional model of the equiaxed grain formation in multi-crystalline silicon, Journal of Crystal Growth, 319 (2011) 106-113.
[65] P. Rudolph, Handbook of Crystal Growth: Bulk Crystal Growth: Basic Techniques, in, 2015, pp. 381-382.
[66] B.K. Voronov, L.D. Dudkin, N.I. Kiryukhina, N.N. Trusova, Cr-Si Phase Diagram Refinment Based on Results of the Growth of Chromium Monosilicide and Disilicide Single Crystals, Izvestiya Akademii Nauk SSSR, Neorganicheskie Materialy, 4 (1968) 58-61.
[67] L.D. Dudkin, E.S. Kuznetsova, Investigation of the electrophysical properties of alloys based on semiconductor disilicides of chromium and manganese., Poroshkovaya Metallurgtya, 6 (1962) 20-31.
[68] K.A. Jackson, Liquid Metals and Solidification, in: Growth and Perfection of Crystals, ASM Cleveland, 1958.
[69] L. Topor, O.J. Kleppa, Standard enthalpy of formation of $CrSi_2$ by high-temperature mixing calorimetry, Journal of Chemical Thermodynamics, 19 (1987) 69-75.
[70] D.M. Herlach, D. Simons, P.Y. Pichon, Crystal growth kinetics in undercooled melts of pure Ge, Si and Ge-Si alloys, Philosophical transactions. Series A, Mathematical, physical, and engineering sciences, 376 (2018).
[71] P. Rudolph, Handbook of Crystal Growth: Bulk Crystal Growth: Basic Techniques, in, 2015, Chap. 9.3.4.
[72] M.A. Martorano, J.B.F. Neto, T.S. Oliveira, T.O. Tsubaki, Refining of metallurgical silicon by directional solidification, Materials Science and Engineering: B, 176 (2011) 217-226.
[73] W. Li, E. Meng, T. Matsushita, S. Oda, D. Ishikawa, K. Nakane, J. Hu, S. Guan, A. Ishida, H. Tatsuoka, Syntheses and structural characterizations of CrSi2 nanostructures using Si substrates under CrCl2 vapor, Journal of Crystal Growth, 365 (2013) 11-18.
[74] K. Seo, K.S.K. Varadwaj, D. Cha, J. In, K. Jiyoung, J. Park, B. Kim, Synthesis and Electrical Properties of Single Crystalline $CrSi_2$ Nanowires, Journal of Physical Chemistry C, 111 (2007) 9072-9076.
[75] K. Fujiwara, Y. Obinata, T. Ujihara, N. Usami, G. Sazaki, K. Nakajima, Grain growth behaviors of polycrystalline silicon during melt growth processes, Journal of Crystal Growth, 266 (2004) 441-448.
[76] T. Duffar, A. Nadri, The grain–grain–liquid triple phase line during solidification of multi-crystalline silicon, Comptes Rendus Physique, 14 (2013) 185-191.
[77] H.K. Lin, C.W. Lan, Revisiting the twinning mechanism in directional solidification of multi-crystalline silicon sheet, Acta Materialia, 131 (2017) 1-10.
[78] R. Obbard, I. Baker, K. Sieg, Using electron backscatter diffraction patterns to examine recrystallization in polar ice sheets, Journal of Glaciology, 52 (2006) 546-557.
[79] B. Beausir, S. Biswas, D.I. Kim, L.S. Tóth, S. Suwas, Analysis of microstructure and texture evolution in pure magnesium during symmetric and asymmetric rolling, Acta Materialia, 57 (2009) 5061-5077.
[80] J. Wheeler, D. Prior, Z. Jiang, R. Spiess, P. Trimby, The petrological significance of misorientations between grains, Contributions to mineralogy and petrology, 141 (2001) 109-124.

Figure captions

Figure 1: a) Silica glass crucible coated with BN b) pBN crucible c) schematic diagram of the VGF growth furnace (1- crucible; 2- graphite holder; 3- carbon heater; 4- bottom thermocouples; 5 – top thermocouple 6- carbon foam insulator; 7- water cooling).

Figure 2: a) Temperature distribution in the furnace as a function of the position of the top of the 40 mm length crucible ○ Bottom thermocouple ● Top thermocouple (marked respectively 4 and 5 on Figure 1-c). The position 0 is taken as the top of the conical carbon heater. b) Temperature program controlled by the bottom thermocouple.

Figure 3: Optical image of ingot (A) to (D).

Figure 4: Optical image of the ingot (A) elaborated in silica glass crucible (right) and backscattered SEM images near the surface of the ingot at different positions (left). The different areas analyzed by EDX are identified from 1 to 5.

Figure 5. Powder X-Ray Diffraction of ingot (A) at the center and at the top of the ingot. Secondary phases are observed and indexed on the top pattern. The phase indexation is made from the ICDD PDF database ($CrSi_2$: 04-016-2861, SiC: 04-008-2393, CrB: 01-089-3587, Cr_5Si_3: 04-001-7859)

Figure 6: Optical and EBSD band contrast (cross-section) images of the ingots (B) and (C). The secondary phases identified by EBSD are colored. The grey parts are indexed to $CrSi_2$.

Figure 7: x direction Inverse Pole Figure (IPF) color maps and pole figure of the ingots (B), (C) and (D). The grain boundaries are indicated in black lines for misorientation above 10° and green lines for misorientation between 2° and 10° (subgrains).

Figure 8: a) Texture analysis by EBSD and b) neutron Laue diffraction pattern of the ingot (B).

Figure 9: Misorientation angle distribution and pole figure for correlated and uncorrelated grains of the ingots (C) (left) and (D) (right) compared to the Mackenzie distribution (x and y axis of Figure 7)

Tables

Table 1: Experimental growth conditions (cooling rate, thermal gradient and growth rate) of 4 ingots grown in 40 and 80 mm length, 7 mm inner diameter crucible in (A) Silica glass (SiO_2) coated with BN, (B) and (D) pBN, (C) pBN treated with HF.

Table 2: Chemical composition of Si, Cr, C and O near the surface of the ingot given by EDX from the five areas, noted 1 to 5 and identified in Figure 4. The Si/Cr ratio is also given in the homogeneous areas.